Soft Matter

Cite this: *Soft Matter*, 2012, **8**, 9101

www.rsc.org/softmatter

PAPER

Stability of peptide (P1 and P2) binding to a graphene sheet *via* an all-atom to all-residue coarse-grained approach†

R. B. Pandey,*[a] Zhifeng Kuang,[b] B. L. Farmer,[b] Steve S. Kim[b] and Rajesh R. Naik[b]

Received 13th April 2012, Accepted 6th July 2012
DOI: 10.1039/c2sm25870f

Peptide binding to a graphene sheet is studied by a coarse-grained approach. All-atom molecular dynamics (MD) is used to assess the adsorption energy (*e.g.* binding) of each amino acid with graphene. The relative adsorption energy of each residue is normalized to describe its coarse-grained interactions with graphene which is used as an input to a phenomenological interaction in an all-residue coarse-grained (ARCG) representation of the peptide chain. Large scale Monte Carlo (MC) simulations are performed to study the stability of peptides (P1: ^{1}H–^{2}S–^{3}S–^{4}Y–^{5}W–^{6}Y–^{7}A–^{8}F–^{9}N–^{10}N–^{11}K–^{12}T and P2: ^{1}E–^{2}P–^{3}L–^{4}Q–^{5}L–^{6}K–^{7}M) binding to a graphene sheet as a function of temperature. A number of local and global physical quantities are analyzed including mobility and substrate-in-contact profiles of each residue, density profiles, root mean square displacement of the center of mass of each peptide and its radius of gyration. We find that P1 has a higher probability of binding to a graphene sheet than P2 supported by both local and global physical quantities. All residues of P1 can bind to the graphene sheet at low temperatures; however, three residues ^{4}Y–^{5}W–^{6}Y seem to anchor it most strongly at higher temperatures, which is consistent with an all-atom MD simulation.

1. Introduction

Fabrication of multifunctional materials with optimal characteristics *via* directed assembly of biofunctionalized nanoparticles has become a subject of immense interest in recent years[1–6] due in part to advances in manipulating structures at nano scales. Peptides are some of the most versatile functionalizing agents with their prolific conformational response and selective binding characteristics. Therefore, identifying peptides that can selectively bind to desirable nano-particles[7–10] (*e.g.*, gold, palladium, clay platelets, *etc.*), including graphitic surfaces,[11] has become one of the major thrusts in designing materials with desirable characteristics; the list of references is too long to cite all here. Kim *et al.*[6] have recently found that peptides P1: ^{1}H–^{2}S–^{3}S–^{4}Y–^{5}W–^{6}Y–^{7}A–^{8}F–^{9}N–^{10}N–^{11}K–^{12}T and P2: ^{1}E–^{2}P–^{3}L–^{4}Q–^{5}L–^{6}K–^{7}M bind selectively to graphene surfaces and edges, which is critical in modulating both the mechanical as well as electronic transport properties of graphene. They have argued that the noncovalent selective binding of peptide to a planar surface or edge of graphene is due to π–π stacking or electrostatic interaction. Such a distinction at the atomic scale was feasible by computer simulation only using an all-atomic model.[6,11] We would like to extend the computer simulation study further on a large scale using a coarse-grained Monte Carlo (MC) simulation with an input from the all-atom molecular dynamics (MD) study at small scales. Our primary goal is to assess the relative binding of peptides P1 and P2, identify the underlying residues that anchor the binding, and evaluate its stability with respect to temperature at equilibrium.

Peptides are assembled from a set of amino acids tethered together in a chain *via* peptide (covalent) bonds. Twenty amino acids (AAs) constitute the basic building blocks of peptides, which range from a molar mass of 75 DA (10 atoms) to 204 DA (27 atoms) with key elements carbon, hydrogen, oxygen, and nitrogen. Each amino acid is characterized by its unique side chain along with an amine and carboxylic acid groups. The degrees of freedom (torsional, covalent elastic bonds, translational) associated with atoms in each amino acid and its assembly in a peptide chain spans a vast conformational phase space. Scanning such a huge set of conformations that characterize specific equilibrium structures requires time steps generally not accessible in all-atom computational modeling[12] particularly in monitoring the large scale structural changes and relaxation of large peptides in appropriate environments. Self and directed assembly of peptides, peptide binding to substrates including biofunctionalization of nano particles, and protein folding in a range of solvent environments may involve multiscale relaxations. Large scale (spatial and temporal) investigation of such complex systems is generally not amenable to computational approaches with atomic resolution. Therefore, some degree of approximation with a lower resolution description is necessary in almost all computer simulation modeling.

[a]*Department of Physics and Astronomy, University of Southern Mississippi, Hattiesburg, MS 39406-0001, USA. E-mail: ras.pandey@usm.edu*
[b]*Materials and Manufacturing Directorate, Air Force Research Laboratory, Wright Patterson Air Force BaseOH 45433, USA*
† Electronic supplementary information (ESI) available. See DOI: 10.1039/c2sm25870f

Reducing the degrees of freedom while preserving the pertinent features of peptides on a large scale is one of the primary objectives in coarse-graining mechanisms. Enormous efforts[13–31] have been directed towards developing coarse-grained models using both Monte Carlo and molecular dynamics methods. Designing appropriate force fields has been one of the major efforts in MD studies.[19–31] Because of the ingenuity of such approaches in preserving the pertinent features, remarkable success is achieved in addressing a number of issues in biomacromolecular assembly. It involves a variety of mechanisms such as setting parameters for an effective residue–residue interaction to achieve conformational relaxation into the native configuration of a protein *via* a reduced model,[15] representing several atomic units of a residue by an effective potential with specific constraints in united residue descriptions,[19] force matching to minimize the difference between atomic and predicted effective forces,[21–23] and so on. For example, using a coarse-grained molecular dynamics simulation, Sorensen *et al.*[29] have examined the assembly of amylin peptides and shown that the "protofibrils are not formed independently in solution but are subunits of the larger growing fibril." They have pointed out the limitations underlying the coarse-grained approaches, namely the time scale is too large to cover the entire relaxation and assembly processes even using the CG models despite the structural constraints and approximate force field.

Computing limitations (both temporal and spatial) are extensively discussed[32] in polymers particularly in complex polymer systems.[33,34] It is not feasible to cover complete polymer chain dynamics (*e.g.*, Rouse, reptation, post-reptation, diffusion from short to long time dynamics of chains in an idealized dense melt). One can hardly approach reptation from short time Rouse dynamics.[35] Thus, reaching the long time diffusion from short time relaxation is out of the question by off-lattice MD simulations even with the coarse-grained (bead–spring) model. Such a long relaxation time for polymer chains in the melt is not accessible by MD simulations due to excessively large degrees of freedom in the continuum (off-lattice) space. The bond-fluctuation description of the polymer chain[32,36] on a discrete lattice with reduced but ample degrees of freedom has become a method of choice for such large scale simulations to study complex macromolecular systems.[33,34] We have already adopted such methods in studying the global properties of proteins[17,18] and peptide binding to specific substrates.[7–9,37,38] In this article, we would like to develop it further with input from an all-atom MD simulation. A peptide can be represented by a chain of coarse-grained nodes where each node represents an amino acid. In addition to ignoring the structural details of amino acids, one of the main issues remaining is how to capture the specificity of the amino acid in its representative node, particularly its interaction with the underlying matrix (graphene). Obviously it depends on the issues to be addressed, for example, the binding of peptides P1 and P2 to a graphene sheet examined here.

The computer simulation is carried out in two steps (bottom-up): (i) consider the binding of each amino acid (a free residue) with the graphene sheet analogous to a recent study by Feng *et al.*[39] on a gold substrate. This will entail performing large-scale simulations with all-atom details of each amino acid and evaluating its binding energy with graphene. This step captures the atomic scale details of the amino acid by the ensemble averaging of its equilibrium structures; the binding energy of an amino acid in equilibrium constitutes its interaction strength with the substrate. (ii) The binding energy of each amino acid is then used as an input to an interaction potential between the coarse-grained peptide node (residue) and the graphene sheet. Simulations with the coarse-grained peptide chain are then carried out for a sufficiently long time to find the relative binding of the peptides and identify the residues that are most likely to anchor them. To assure that the results obtained for the binding of peptides from the coarse-grained approach are reliable, we carried out simulation for a simplified system first, such as a peptide chain in a simulation box with a graphene sheet by the all-atom approach and see if the same results are recovered by the coarse-grained model. In the following we describe the all-atom procedure and how its results are used in our coarse-grained approach. Large scale results are presented in the subsequent section followed by a summary and conclusion.

2. All-atom approach

Using an all-atom representation of the amino acids, molecular dynamics (MD) simulations were performed to estimate the relative binding of all twenty amino acids to a graphene sheet. The relative binding affinity is quantified by the adsorption energy. Here we define the adsorption energy as the minimum interaction energy between an amino acid and a model graphene sheet after the system is equilibrated. Since a neutral rigid graphene sheet was used in our calculations, the interaction energy only accounts for the van der Waals potential energy between an amino acid and the model graphene sheet.

The reliability of the adsorption energy calculations depends on force fields as demonstrated by Collier *et al.*[40] Since the commonly used force fields are developed in aqueous solution, their transferability to interfacial interaction is questionable.[41,42] However, two recent molecular dynamics simulations[6,43] have shown that Amber force field ff99SB can be used to reproduce the secondary structures of peptides comparable to experimental measurements when the peptides are adsorbed on a graphene sheet. The predicted peptide secondary structures correspond to the minimum interaction energy (adsorption energy). Therefore we employed Amber force field ff99SB to calculate the adsorption energy of the 20 amino acids on a graphene sheet as an input to large scale coarse-grained Monte Carlo simulations.

The model graphene sheet is of the size 5 nm × 5 nm. The surface carbons of the graphene sheet are modeled as sp2 hybrids while the unsaturated carbon atoms on the edges are terminated with hydrogen atoms. The center of mass of the backbone atoms of an amino acid is initially located at 1 nm above the graphene ribbon center using an in-house developed code (Fig. 1). To avoid forming a possible salt bridge between the termini, each residue is capped using acetyl (ACE) and amine (NME) groups. When it is necessary, Na^+ or Cl^- ions are added to neutralize the system. For each amino acid, ten independent simulations were performed using different initial atomic velocities in vacuum phase using NAMD software.[44] Each simulation equilibrated for 40 ns. The adsorption energy for each amino acid was obtained using the last 1000 snapshots taken every 10 ps along each of the ten trajectories. The obtained adsorption energy in vacuum phase is listed in the third column in Table 1 and shown in Fig. 2.

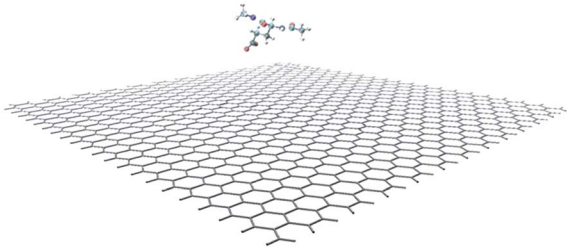

Fig. 1 The initial configuration of an amino acid above a graphene ribbon.

Since only van der Waals interaction is included in the calculated adsorption energy, all the calculated adsorption energies are negative. The calculated adsorption energies show that the first six strong binders are TRP (−23.4 kcal mol^{-1}), TYR (−20.3 kcal mol^{-1}), ARG (−19.3 kcal mol^{-1}), PHE (−18.1 kcal mol^{-1}), HIS (−17.0 kcal mol^{-1}), and LYS (−15.5 kcal mol^{-1}). The predicted binding order TRP > TYR > PHE > HIS is consistent with the prediction of the density functional theory for the relative binding of these amino acids to graphene with binding energies of 9.7 kcal mol^{-1} (tryptophan), 7.1 kcal mol^{-1} (tyrosine), 5.8 kcal mol^{-1} (phenylalanine), and 4.8 kcal mol^{-1} (histidine).[45] The relative binding affinity has also been verified by experiments.[46] Therefore it is reasonable to use these data further in coarse-grained Monte Carlo simulations.

To test the water effect, the equilibrated systems with minimum interaction energy were solvated in water. Water molecules surround the system extending 1.2 nm away from the solute in all three dimensions. After minimization and gradually heating the system up to 300 K, 40 ns equilibration was performed in an NVT ensemble using 3-D periodic boundary conditions. The particle-mesh Ewald (PME) method was used for the long-range electrostatic interaction calculations. A smooth switching function was used to truncate the van der Waals potential energy smoothly at the cutoff distance of 1.2 nm and switch distance of 1.0 nm. As in the vacuum phase, the adsorption energy was calculated using the last 1000 snapshots taken every 10 ps along each of the ten trajectories. The calculated adsorption energy in the water phase is listed in the fourth column in Table 1. The difference of all the calculated adsorption energies between those in-vacuum and in-water is less than 1.5 kcal mol^{-1}. This implies that the van der Waals interaction is the dominant force for the adsorption. The last column of the table is the relative adsorption energy normalized by the largest value in the table.

Table 1 Amino acids with their hydropathy index (hydrophobic (H), polar (P), and electrostatic (E) groups), adsorption energy (ΔE) and its normalized values

		ΔE (MD) (kcal mol^{-1})			
Amino acid	H/P/E	Vacuum	Water	Difference	Normalized
Ile (I): H_1	4.5	−14.1	−13.3	0.8	−0.567
Val (V): H_2	4.2	−12.2	−11.7	0.5	−0.519
Leu (L): H_3	3.8	−14.2	−13.5	0.7	−0.599
Phe (F): H_4	2.8	−18.1	−18.4	0.3	−0.701
Cys (C): H_5	2.5	−11.5	−11.2	0.3	−0.487
Met (M): H_6	1.9	−15.2	−15.4	0.2	−0.626
Ala (A): H_7	1.8	−9.3	−9.0	0.3	−0.380
Gly (G): H_8	−0.4	−7.8	−7.7	0.1	−0.348
Thr (T): P_1	−0.7	−12.0	−12.0	0.0	−0.497
Ser (S): P_2	−0.8	−10.7	−10.4	0.3	−0.412
Trp (W): P_3	−0.9	−23.4	−23.6	0.2	−1.000
Tyr (Y): P_4	−1.3	−20.3	−18.9	1.4	−0.856
Pro (P): P_5	−1.6	−12.0	−11.5	0.5	−0.460
His (H): P_6	−3.2	−17.0	−15.9	1.1	−0.759
Gln (Q): P_7	−3.5	−15.3	−16.1	0.8	−0.658
Asn (N): P_8	−3.5	−13.2	−13.6	0.4	−0.588
Asp (D): E_1	−3.5	−12.2	−11.2	1.0	−0.497
Glu (E): E_2	−3.5	−13.4	−15.1	1.7	−0.561
Lys (K): E_3	−3.9	−15.5	−16.5	1.0	−0.572
Arg (R): E_4	−4.5	−19.3	−20.1	0.8	−0.690

It is worth exploring the binding of peptides P1 and P2 by all-atom MD simulation first. The structures of P1 and P2 predicted by Kim *et al.*[6] were used as initial structures in this study. Each peptide (P1 and P2) was manually placed at five different starting positions relative to the rigid 5 × 5 nm graphene sheet: one close to the zigzag edge, one close to the arm chair edge, one close to the surface, and one at a distance away from the surface. Each simulation system consists of a peptide, a graphene sheet and necessary neutralization ions. Fig. 3 shows the five starting positions of P2 in five different simulation settings as an example. For each system, we performed 2 independent MD simulations using different initial velocities. Each simulation was done for 100 ns. 1000 trajectory snapshots taken every 10 ps in the last 10 ns were used to calculate the interaction energy between an individual residue and the graphene sheet. The calculated adsorption energies are shown in Fig. 4. The strong binding

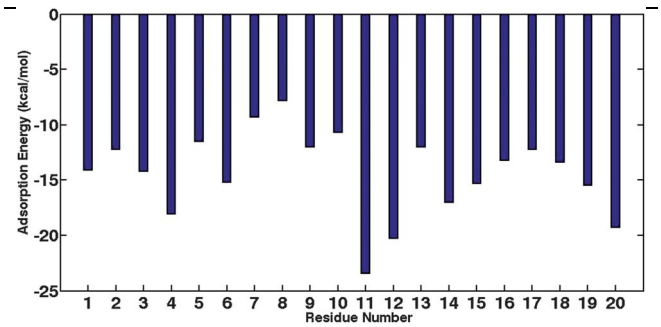

Fig. 2 Adsorption energy of each amino acid: ^{1}I–^{2}V–^{3}L–^{4}F–^{5}C–^{6}M–^{7}A–^{8}G–^{9}T–^{10}S–^{11}W–^{12}Y–^{13}P–^{14}H–^{15}Q–^{16}N–^{17}D–^{18}E–^{19}K–^{20}R from all-atom MD simulation (Table 1).

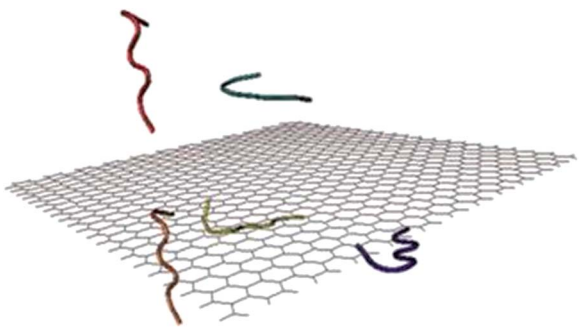

Fig. 3 Overlap view of initial configurations of P2 peptide in five simulations.

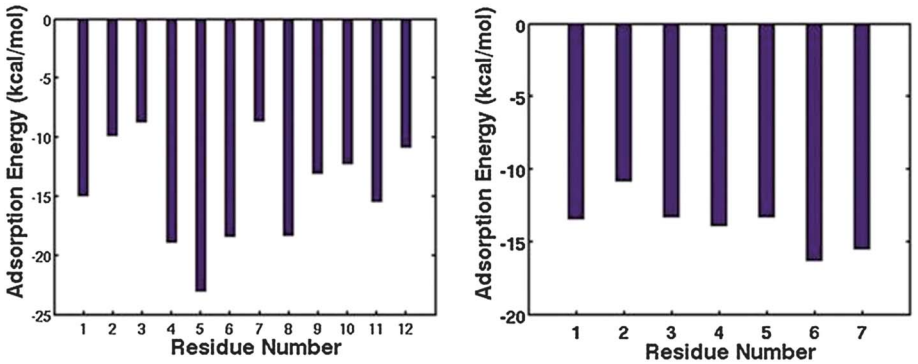

Fig. 4 The interaction energies (kcal mol^{-1}) of individual residues with the graphene sheet (binding energy) of peptides P1 (^{1}H–^{2}S–^{3}S–^{4}Y–^{5}W–^{6}Y–^{7}A–^{8}F–^{9}N–^{10}N–^{11}K–^{12}T) and P2 (^{1}E–^{2}P–^{3}L–^{4}Q–^{5}L–^{6}K–^{7}M).

residues are ^{4}Y–^{5}W–^{6}Y⋯^{8}F for P1 as clearly seen in Fig. 4. This is in agreement with the results from Kim *et al.*[6] in explicit water simulation and Rajesh *et al.*[45] in density functional theory calculation. This is not surprising because pi–pi interaction can be resolved in vacuum phase. For P2, there is no strong binding motif to the surface. This is again in agreement with Kim *et al.*'s observation that P2 prefers to bind to the edge due to electrostatic interaction.[6]

3. All-residue coarse-grained approach

As mentioned above, a peptide is described by a set of nodes tethered together *via* peptide (covalent) bonds, where a node represents an amino acid. The peptide P1 (^{1}H–^{2}S–^{3}S–^{4}Y–^{5}W–^{6}Y–^{7}A–^{8}F–^{9}N–^{10}N–^{11}K–^{12}T) is a chain of twelve nodes and P2 (^{1}E–^{2}P–^{3}L–^{4}Q–^{5}L–^{6}K–^{7}M) is a chain of seven nodes. The internal structure of the amino acid is ignored but its unique characteristics are captured by specific coarse-grained interaction(s) (as follows).

We consider the peptide chains and the graphene sheet on a cubic lattice. A node occupies a cube (eight lattice sites) and the bond length between consecutive nodes can vary (fluctuate) between 2 and $\sqrt{10}$ in units of lattice constant. The bond fluctuation description on a cubic lattice is known[32] to incorporate ample degrees of freedom while enhancing the computational efficiency. Such bond fluctuation methods are extensively used in investigating the structure and dynamics of complex polymer systems, multi-component nano-composites,[7,9] and protein chains.[17,18] Each node of the peptide chains interacts with the neighboring nodes and the substrate (graphene) sites with a generalized Lennard-Jones potential,

$$U_{ij} = \left[|\varepsilon_{ij}| \left(\frac{\sigma}{r_{ij}}\right)^{12} + \varepsilon_{ij} \left(\frac{\sigma}{r_{ij}}\right)^{6} \right], r_{ij} < r_c \qquad (1)$$

where r_{ij} is the distance between the residues at sites i and j, $r_c = \sqrt{8}$ is the range of interaction and $\sigma = 1$ in units of lattice constant. The potential strength ε_{ij} (a measure of the depth) is unique for the interaction of each residue (node) with the substrate and residue–residue interactions pair with appropriate positive (repulsive) and negative (attractive) values. Since we are focused on the binding of peptides to graphene, the interaction between each residue (node) of the peptide and the substrate is critical. We use the binding energy of each residue (Table 1) evaluated from an all-atom simulation as an input where ε_{ij} is the normalized interaction strength.

Specificity of residue–residue interaction is captured *via* a generalized interaction strength[7] based on the hydrophobic, polar, and electrostatic characteristics weighted by its hydropathy index (Table 1). The interactions between polar–polar (ε_{PP}) and polar–electrostatic (ε_{PE}) residue groups are $\varepsilon_{PP} = \varepsilon_{PE} = -0.2$ while the interactions between the electrostatic residues are $\varepsilon_{E2E2} = \varepsilon_{E3E3} = 0.1$ and $\varepsilon_{E2E3} = -0.4$, which are then weighted *via* the hydropathy index (Table 1); these values are selected based on our previous investigations.[7,9] At dilute concentrations of peptides, however, the residue–graphene interactions are more important in assessing the binding than the residue–residue interactions. As pointed out above, our goal is to identify the residues that anchor the binding of peptides P1 and P2 to the graphene sheet.

The graphene sheet is placed at the center. Peptide chains with a concentration C_p are randomly distributed in the simulation box initially. The Metropolis algorithm is used to move each tethered residue (node) randomly as follows.[7,9] A residue at a site i is selected randomly to move to a randomly selected neighboring lattice site j. As long as the excluded volume constraints and the limitations on changes in the covalent bond length are satisfied, the residue is moved from site i to site j with the Boltzmann probability $\exp(-\Delta E_{ij}/T)$, where ΔE_{ij} is the change in energy between its new (E_j) and old (E_i) configurations $\Delta E_{ij} = E_j - E_i$ and T is the temperature in reduced units of the Boltzmann constant and the energy (ε_{ij}). Attempts to move each residue once defines a unit Monte Carlo step (MCS). Parameters and variables (*e.g.*, interaction energy, time) are generally in arbitrary units for identifying the trends, *i.e.*, the changes in variation of the observables. The order of magnitude of these parameters (*e.g.*, energy, time) in a realistic unit can be estimated from the units of the all-atom simulations. Note that the equilibrium values of the adsorption (binding) energy of each residue from the all-atom approach are used here as an input (see above). Therefore, the relaxation time required for an amino acid to reach equilibrium can be considered as a unit for time. The maximum value of the adsorption energy, the normalizing factor in the all-atom approach (see Table 1), can be a unit for energy. Thus, the MCS time step t is of the order of magnitude $t \times$ (time required to relax a residue $\approx$ 40 ns) and the binding energy is

scaled by the normalized factor (18.7 kcal mol^{-1}). In order to identify the relative binding, it is easier to work with the arbitrary unit (in the following) to monitor the variations of the physical quantities.

We consider dilute concentrations of peptides (C_p = 0.001, 0.002) to avoid interpeptide clustering and to allow peptide binding to be more visible. The graphene sheet is fixed but the residues and therefore peptides execute their stochastic motion. Simulations are performed for a sufficiently long time to assess the probability of adsorption of peptides P1 and P2 to the graphene sheet. We know from all-atom simulations (section 2) that interaction between each amino acid (node) and the graphene is attractive. Therefore, each node of both peptides can bind to graphene in an appropriate span of time at least at low temperatures. On the other hand, peptides can be desorbed (unbind) on raising the temperature to a sufficiently high value. In order to distinguish relative binding of P1 and P2, we need to vary temperature systematically and analyze the snapshots and data for the physical quantities accordingly. We have examined a number of local and global physical quantities such as binding energy of each residue in each peptide, its mobility profiles, binding profiles (*i.e.*, the number of graphene sites around each residue), variation of the root mean square (RMS) displacement of the center of mass of each peptide and the radius of gyration with the time steps. The simulations are carried out for a million time steps with 100 independent samples to evaluate these quantities. Qualitative behavior of peptide binding remains unaffected by the sample size; data presented here are generated on a 100^3 lattice with a 24^2 sheet at the center.

4. Results and discussion

Using the bottom-up coarse-grained procedure described above, simulations are carried out for a million time steps on a 100^3 lattice at temperatures T = 0.01–0.04 with the graphene sheet immersed in a dilute solution of peptides (C_p = 0.001). During the course of simulations, stochastic motion of peptide chains and residues, conformational fluctuations, binding and unbinding are monitored *via* animations at each temperature. Fig. 5 shows typical snapshots at the end of a million time steps at different temperatures. Visual inspections of these snapshots (along with animations) show that all peptides (P1 and P2) in each sample bind to the graphene sheet at the low temperature T = 0.01. Raising the temperature leads to a decrease in binding of both peptides with almost no binding at high temperatures. However, binding of peptide P1 is sustained more than that of P2 at higher temperatures (*e.g.*, $T \geq 0.03$).

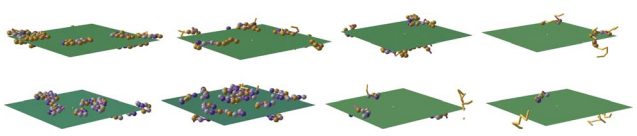

Fig. 5 Snapshots of peptides and the graphene sheet at the end of 10^6 time steps on a 100^3 lattice at temperatures T = 0.01, 0.02, 0.03, and 0.04 from left to right with peptides P1 (top row) and P2 (bottom row). Residues (nodes) within the range of interaction of the sheet are shown as spheres and those beyond the range but part of the chains are not shown for clarity. In color: red, golden, and blue refer to hydrophobic, polar, and electrostatic residues, respectively (see Table 1).

The stochastic dynamics of a free chain or a particle in an asymptotic time limit is diffusive. As the residues (and therefore peptides) execute their stochastic movements and bind to the graphene sheet, their motion is expected to slow down from its diffusive dynamics (before binding). The global dynamics of peptide chains can be identified from the dependence of the root mean square displacement of its center of mass (R_c) on the time steps (t), *i.e.*, $R_c \propto t^{\nu}$ with the exponent ν = ½ for diffusion. Variation of the RMS displacement of the center of mass (R_c) of peptides with the time steps is presented in Fig. 6. From the R_c *versus* t plot on the log–log scale, we see that both peptides (P1 and P2) continue to diffuse at a high temperature (T = 0.04). On lowering the temperature (T = 0.01, 0.02), peptides still diffuse for up to $t \approx 10^5$ steps until they bind to the graphene sheet. As a result peptides slow down and the variation of R_c tapers off in the long (asymptotic) time limit. This shows that simulations should be carried out for a million time steps to identify the binding of peptides to the graphene sheet. At a high temperature (T = 0.04), peptides do not bind despite being in contact with the graphene sheet for a long time. In the log scale, it is difficult to distinguish which peptide, P1 or P2, slows down more (as a result of its binding) in a long time at low temperatures. However, the variation of R_c with t plot on a normal scale (see the inset figure) shows that P1 tends to move slower than P2 which implies that P1 has a higher probability of binding to the graphene sheet than P2.

The interaction energy and adsorption energy of free residues are already evaluated using all-atom simulations (eqn (1), Fig. 2, Table 1) as well as a part of the peptide (Fig. 4). When a set of residues are tethered together in a peptide chain (P1 and P2), the energy of a peptide is not necessarily the sum of energies of its individual residues in their free state. In fact the energy of a peptide chain depends on its conformation and sequence. Thus, the total energy of a residue in a chain can differ from that in its free state (Fig. 2 and 4). Interaction of each residue along with the steric constraints imposed by peptide bonds is very important in controlling the conformation of the peptide chain. We evaluate the average energy E_n (sum of residue–residue and residue–sheet) of each residue in steady-state equilibrium in our coarse-grained

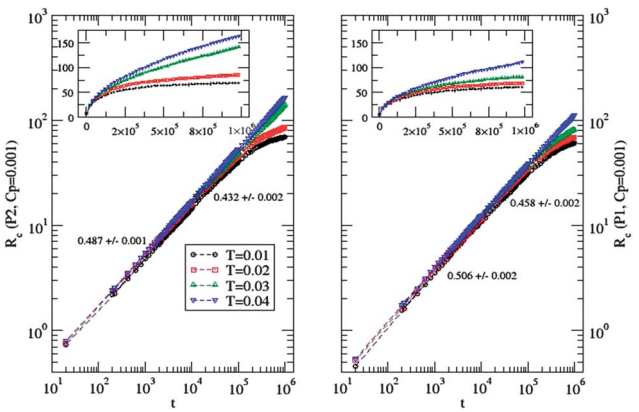

Fig. 6 Variation of the root mean square displacement R_c of peptides P1 and P2 with the time steps t on a log–log scale and normal scale (inset) at temperatures T = 0.01, 0.02, 0.03, and 0.04. Slopes of the data at T = 0.01, at a small time and longer time intervals are included for guidance. Peptide concentration C_p = 0.001, 100^3 lattice, 100 independent samples for the time steps $t = 10^6$.

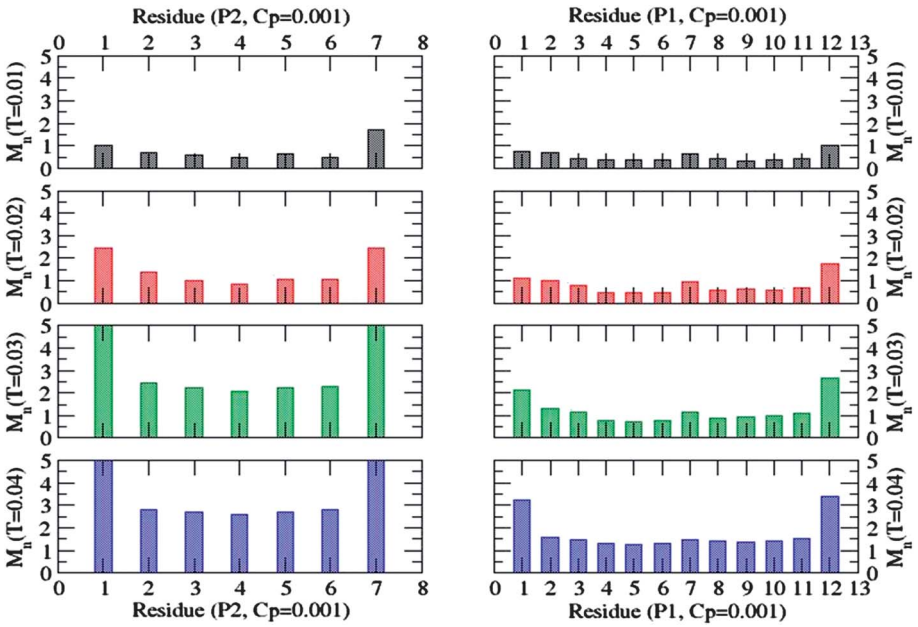

Fig. 7 Mobility of each residue at temperatures $T = 0.01$, 0.02, 0.03, and 0.04 in P1: ^{1}H–^{2}S–^{3}S–^{4}Y–^{5}W–^{6}Y–^{7}A–^{8}F–^{9}N–^{10}N–^{11}K–^{12}T and P2: ^{1}E–^{2}P–^{3}L–^{4}Q–^{5}L–^{6}K–^{7}M. Peptide concentration $C_p = 0.001$, 100^3 lattice, 100 independent samples for the time steps $t = 10^6$.

approach in both peptide chains (P1 and P2) at $T = 0.01$–0.04. We find that the residues ^{10}N and ^{12}T in peptide P1 have the lowest energy; the residue with the lowest energy in P2 is ^{2}P. The energy of these residues decreases with increasing temperature, which implies that the equilibrium conformations of peptides are more stable at higher temperatures. It is, however, not feasible to identify residues that can bind to the graphene sheet from these datasets. In the following we describe the mobility and substrate-in-contact profiles which suggest that these low energy residues do not anchor as much as others in binding the peptides.

Let us look at the relative mobility of each residue. The average number of successful moves per unit time step of each residue is defined as a measure of its mobility. The mobility of each residue (M_n) in both peptides P1 and P2 is presented in Fig. 7 at temperatures $T = 0.01$–0.04. Apart from the end residues (which are less constrained by the covalent bonds than the interior residues), the mobility of residues in P2 is generally higher than that in P1. We know that the mobility of a residue decreases upon its binding to the graphene sheet. The lower mobility of residues (in P1 compared to P2) implies a higher

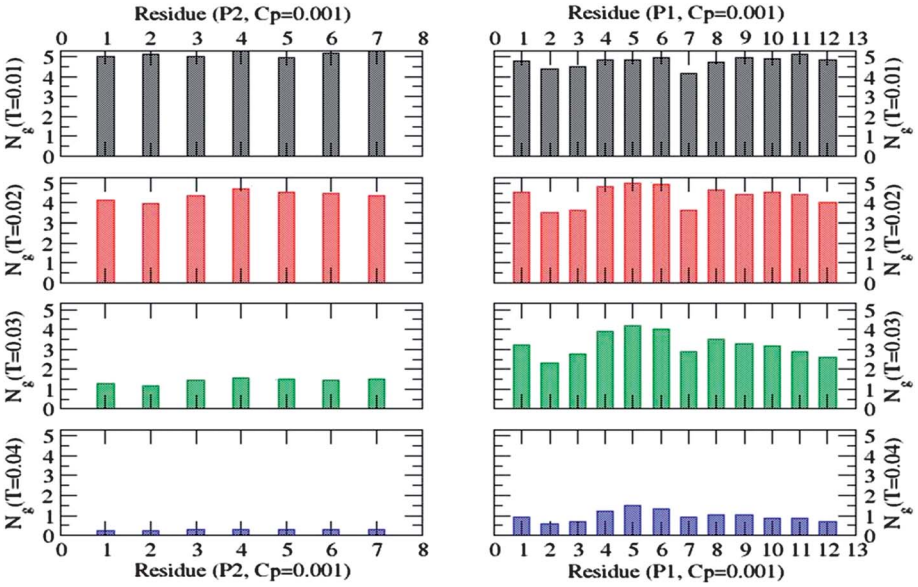

Fig. 8 Substrate-in-contact profiles (N_g) of each residue at temperatures $T = 0.01$, 0.02, 0.03, and 0.04 in P1: ^{1}H–^{2}S–^{3}S–^{4}Y–^{5}W–^{6}Y–^{7}A–^{8}F–^{9}N–^{10}N–^{11}K–^{12}T and P2: ^{1}E–^{2}P–^{3}L–^{4}Q–^{5}L–^{6}K–^{7}M. Peptide concentration $C_p = 0.001$, 100^3 lattice, 100 independent samples for the time steps $t = 10^6$.

probability of its binding. As expected, the mobility of the residues increases with increasing temperature.

The average number of graphene constituents (N_g) around each residue within the range of interaction in the steady-state equilibrium is a measure of its binding probability, *i.e.*, the larger the number of substrate sites to be adsorbed, the stronger the binding. The substrate-in-contact (N_g) profiles of residues in both peptides are presented in Fig. 8 at temperatures $T = 0.01$–0.04. We know that the graphene substrate attracts each residue in both peptides, some more than others (see Fig. 2, Table 1). Therefore almost all residues are expected to be adsorbed onto the graphene sheet at low temperatures ($T = 0.01$, 0.02) which is clearly seen in Fig. 7 (also in snapshots, Fig. 3 and animations). The difference in adsorption of residues in these peptides becomes apparent on raising the temperature to $T = 0.03$ where the number of substrate-in-contact N_g of residues in P1 is substantially (two to four times) higher than that in P2. One may immediately draw the conclusion that P1 is likely to bind to the graphene sheet more strongly than P2. The trend for the difference in adsorption continues on further increasing the temperature although residues in both peptides become more desorbed. All residues in P1 can bind to the graphene sheet with about the same strength; three residues, ^{4}Y–^{5}W–^{6}Y, seem to anchor it most strongly. These findings are consistent with the estimates of their binding energies in the all-atom simulation (Fig. 4).

Density profiles of peptides in the longitudinal (x, z) and transverse (y, normal to sheet) directions are also analyzed (see Fig. 9). Density of each component is calculated from the number of lattice sites occupied by its constituents (P1, P2, or sheet) divided by the total number of sites (L^2) in each plane. It is difficult to identify which peptide (P1 or P2) binds more to edges than the surfaces of the graphene sheet due to lack of structural

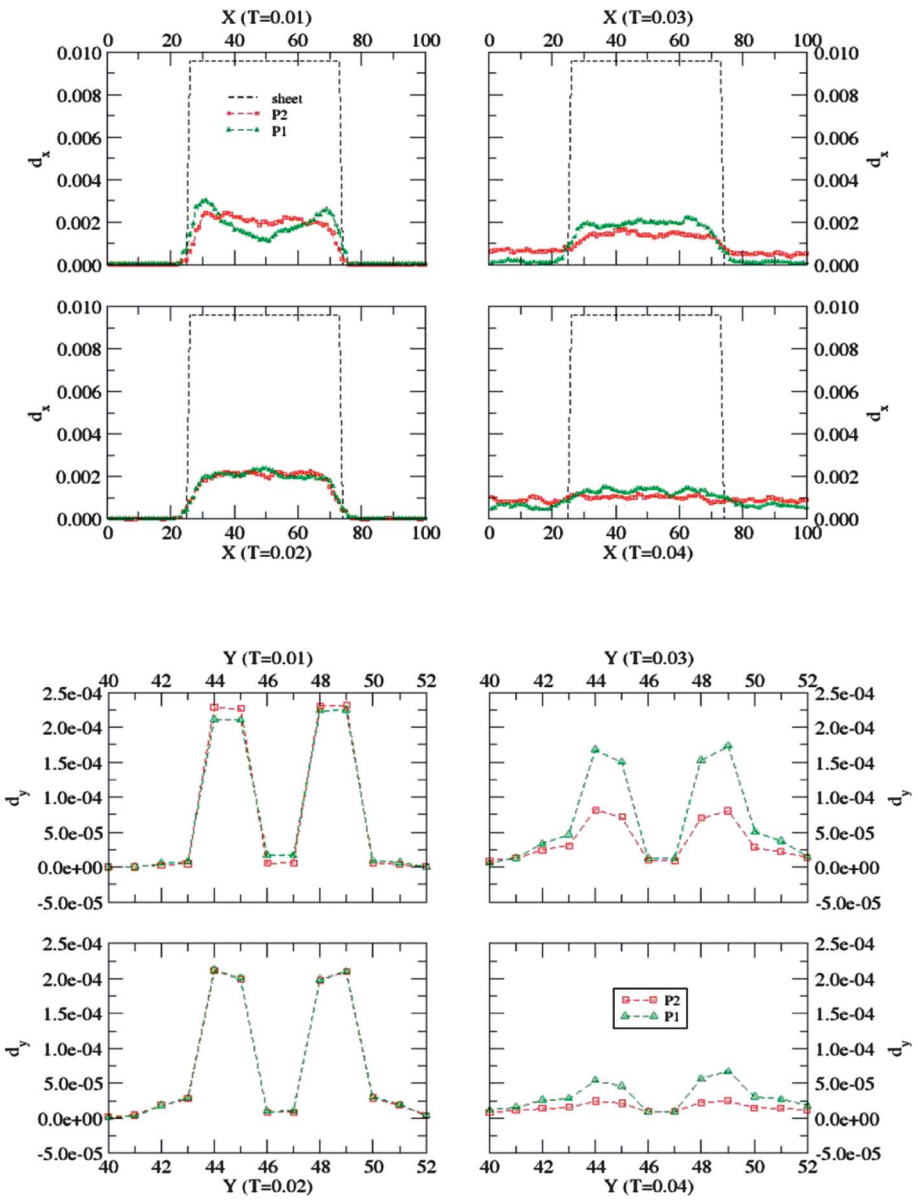

Fig. 9 Longitudinal (x, top) and transverse (y, bottom) density profiles of the peptide. The density of the sheet is included in the longitudinal density profiles. Statistics is the same as in Fig. 7 and 8.

details at the atomic scale. For example, the visual inspections with the coarse-grained model (*e.g.* Fig. 5) do not show such distinction. Such a distinction between the structures on the edges and surfaces and associated bonding with the amino acids can be made using all-atom simulations[6] with the atomic resolution: P2 as an edge binding peptide *versus* P1 as the surface binding peptide. The effect of temperature on the equilibrium adsorption and desorption can however be verified from the density profiles (Fig. 9). The density of P2 is more homogeneously distributed around the sheet than that of P1 which seems to be more concentrated around edges at the low temperature $T = 0.01$ (longitudinal density profile). Since P1 is larger than P2, adsorption of P1 to the edges may be due to morphological constraints rather than the interaction with the sheet. Such a distinction cannot be made from the transverse component of the density profile (Fig. 9). Raising the temperature leads to homogenization of peptide distribution around the sheet with peptide P1 binding more strongly than P2 (transverse density profile at $T = 0.03$, 0.04 in Fig. 9).

We have also examined the effect of temperature on the size of the peptides as they bind and unbind to the graphene sheet. The variation of the radius of gyration and its components (see the ESI, Fig. S1 and S3† for the transverse component in particular) with the temperature shows how it elongates, a signature of unbinding, on raising the temperature. The transverse (y) component (normal to the sheet) decays with the time steps before reaching its steady-state value; the rate of decay increases on reducing the temperature as their binding. The thermal response of the radius of gyration of P1 differs from that of P2 (Fig. S2 and S3†) which supports our observations discussed above, *i.e.*, the probability of P1 binding to graphene is higher than that of P2.

5. Summary and conclusions

A coarse-grained approach with an all-atom to all-residue description is used in hierarchy to investigate binding of peptides P1 and P2 to a graphene sheet in asymptotic (long time) equilibrium. We consider the adsorption (binding) of amino acids (one at a time) onto a graphene sheet with all-atom details of each component. Large scale MD simulations are performed to evaluate the adsorption energy of each amino acid, which is a measure of binding affinity. The relative binding energy of each amino acid is then used as an input in a generalized LJ potential for the all-residue coarse-grained approach. In the coarse-grained description, a peptide is described by a set of nodes tethered together *via* covalent bonds, where a node represents an amino acid. The internal structure of the amino acid is thus averaged out in the all-atom approach but its unique characteristics are captured by specific interaction(s) composed from the all-atom simulations.

We have examined a number of local and global physical quantities such as binding energy of each residue in each peptide, mobility profiles, binding profiles (*i.e.*, the number of graphene sites around each residue), variation of the root mean square displacement of the center of mass of each peptide and the radius of gyration with the time steps. We find that at low temperatures both peptides (P1 and P2) can bind to the graphene sheet and unbind on raising the temperature with almost no binding at high temperature as expected. The variation of the RMS displacement of the peptide R_c with the time step t (analysis of a global quantity) shows that P1 tends to move slower than P2, which implies that P1 has a higher probability of binding to the graphene sheet than P2. These trends are consistent with the analysis of other global quantities as well, such as radius of gyration and density profiles.

Analysis of physical quantities such as mobility and substrate-in-contact profiles of each residue provides insight into the binding of residues. We find that all residues are adsorbed onto the graphene sheet at low temperatures ($T = 0.01$, 0.02) as expected. The difference in adsorption of residues in these peptides appears on raising the temperature to $T = 0.03$ where the number of substrate-in-contact N_g of residues in P1 is substantially (two to four times) higher than that in P2. Thus, P1 is likely to bind more strongly to the graphene sheet than P2. All residues in P1 can bind to the graphene sheet with similar strength; however, three residues, ^{4}Y–^{5}W–^{6}Y, seem to anchor it most strongly, which is consistent with the all-atom MD simulations.

A two step hierarchical coarse-grained approach presented here involves all-atom descriptions with off-lattice MD to capture small-scale details and are used as an input to all-residue CGMC on a lattice to span large-scales. Such an approach would be useful in investigating more complex systems such as a mixture of protein, membranes, and solvent, a subject of our ongoing effort.

Acknowledgements

This work is supported by the Air Force Research Laboratory. We thank Diana Lovejoy for careful reading of the manuscript and corrections and referees for constructive criticism.

References

1 S. R. Whaley, D. S. English, E. L. Hu, P. F. Barbara and A. M. Belcher, Selection of peptides with semiconductor binding specificity for directed nanocrystal assembly, *Nature*, 2000, **405**, 665–668.
2 M. Sarikaya, C. Tamerler, A. K. Y. Jen, K. Schulten and F. Baneyx, Molecular biomimetics: nanotechnology through biology, *Nat. Mater.*, 2003, **2**, 577–585.
3 Y. Fang, Q. Wu, M. B. Dickerson, Y. Cai, S. Shian, J. D. Berrigan, N. Poulsen, N. Kroger and K. H. Sandhage, Protein-mediated layer-by-layer syntheses of freestanding microscale titania structures with biologically assembled 3-D morphologies, *Chem. Mater.*, 2009, **21**, 5704–5710.
4 M. J. Pender, L. A. Sowards, J. D. Hartgerink, M. O. Stone and R. R. Naik, Peptide-mediated formation of single-wall carbon nanotube composites, *Nano Lett.*, 2006, **6**, 40–44.
5 Y. Cui, S. N. Kim, S. E. Jones, L. L. Wissler, R. R. Naik and M. C. McAlpine, Chemical functionalization of graphene enabled by phage displayed peptides, *Nano Lett.*, 2010, **10**, 4559–4565.
6 S. N. Kim, Z. Kuang, J. M. Slocik, S. E. Jones, Y. Cui, B. L. Farmer, M. C. McAlpine and R. R. Naik, Preferential binding of peptides to graphene edges and planes, *J. Am. Chem. Soc.*, 2011, **133**, 14480–14483.
7 R. B. Pandey, *et al*, Adsorption of peptides (A3, Flg, Pd2, Pd4) on gold and palladium surfaces by a coarse-grained Monte Carlo simulation, *Phys. Chem. Chem. Phys.*, 2009, **11**, 1989–2001.
8 H. Heinz, *et al*, Molecular interactions of peptides with gold, palladium, and Pd–Au bimetal surfaces in aqueous solution, *J. Am. Chem. Soc.*, 2009, **131**, 9704–9714.
9 R. B. Pandey, *et al*, A layer of clay platelets in a peptide (M1: HGINTTKPFKSV) matrix: binding, encapsulation and

morphology, *J. Polym. Sci., Part B: Polym. Phys.*, 2010, **48**, 2566–2574.
10 L. F. Drummy, *et al*, Bioassembled layered silicate–metal nanoparticle hybrids, *ACS Appl. Mater. Interfaces*, 2010, **2**, 1492–1498.
11 S. M. Tomasio and T. R. Walsh, Modeling the binding affinity of peptides for graphitic surfaces. Influences of aromatic content and interfacial shape, *J. Phys. Chem.*, 2009, **113**, 8778–8785.
12 P. L. Freddolino, C. B. Harrison, Y. Liu and K. Schulten, Challenges in protein folding simulations: timescale, representation, and analysis, *Nat. Phys.*, 2010, **6**, 751–758.
13 A. P. Lyubartsev and A. Laaksonen, Calculation of effective interaction potentials from radial distribution functions: a reverse Monte Carlo approach, *Phys. Rev. E: Stat. Phys., Plasmas, Fluids, Relat. Interdiscip. Top.*, 1995, **52**, 3730–3737.
14 J. Zhou, S. Chen and S. Jiang, Orientation of adsorbed antibodies on charged surfaces by computer simulation based on a united-residue model, *Langmuir*, 2003, **19**, 3472–3478.
15 A. E. van Giessen and J. E. Straub, Mote Carlo simulations of polyalanine using a reduced model and statistics-based interaction potential, *J. Chem. Phys.*, 2005, **122**, 0249041–0249049.
16 D. Reith, M. Putz and F. Muller-Plathe, Deriving effective mesoscale potentials from atomistic simulations, *J. Comput. Chem.*, 2003, **24**, 1624–1636.
17 R. B. Pandey and B. L. Farmer, Conformation of a coarse-grained protein chain (an aspartic acid protease) model in effective solvent by a bond-fluctuating Monte Carlo simulation, *Phys. Rev. E: Stat., Nonlinear, Soft Matter Phys.*, 2008, **77**, 031902–031910.
18 R. B. Pandey and B. L. Farmer, Global structure of a human immunodeficiency virus-1 protease (1DIFA dimer) in an effective solvent medium by a Monte Carlo simulation, *J. Chem. Phys.*, 2010, **132**, 125101–125106.
19 A. Liwo, C. Czaplewski, J. Pillardy and H. A. Scheraga, Cumulant-based expressions for the multibody terms for the correlation between local and electrostatic interactions in the united-residue force field, *J. Chem. Phys.*, 2001, **115**, 2323–2347.
20 A. Liwo, C. Czaplewski, S. Oldziej and H. A. Scheraga, Computational techniques for efficient conformational sampling of protein, *Curr. Opin. Struct. Biol.*, 2008, **18**, 134–139.
21 F. Ercolessi and J. Adams, Interatomic potentials from first-principle calculations: the force-matching method, *Europhys. Lett.*, 1994, **26**, 583–588.
22 J. Zhou, I. F. Thorpe, S. Izvekov and G. A. Voth, Coarse-grained peptide modeling using a systematic multiscale approach, *Biophys. J.*, 2007, **92**, 4289–4303.
23 S. J. Marrink and A. E. Mark, molecular dynamics simulation of the formation, structure, and dynamics of small phospholipid vesicles, *J. Am. Chem. Soc.*, 2003, **125**, 15233–15242.
24 S. J. Marrink and A. E. Mark, The mechanism of vesicle fusion as revealed by molecular dynamics simulations, *J. Am. Chem. Soc.*, 2003, **125**, 11144–11145.
25 S. J. Marrink, A. H. de Vries and A. E. Mark, Coarse-grained model for semi-quantitative lipid simulations, *J. Phys. Chem. B*, 2004, **108**, 750–760.
26 S. J. Marrink, H. J. Risselada, S. Yefimov, D. P. Tieleman and A. H. de Vries, The MARTINI forcefield: coarse-grained model for biomolecular simulations, *J. Phys. Chem. B*, 2007, **111**, 7812–7824.
27 L. X. Peng, L. Yu, S. B. Howell and D. A. Gough, Aggregation properties of a polymeric anticancer therapeutic: a coarse-grained modeling study, *J. Chem. Inf. Model.*, 2011, **51**, 3030–3035.
28 Z. Wu, Q. Cui and A. Yethiraj, A new coarse-grained force field for membrane-peptide simulations, *J. Chem. Theory Comput.*, 2011, **7**, 3793–3802.
29 J. Sorensen, P. Xavier, K. K. Skeby, S. J. Marrink and B. Schiott, Protofibrillar assembly towards the formation of amyloid fibrils, *J. Phys. Chem. Lett.*, 2011, **2**, 2385–2390.
30 K. R. Hadley and C. McCabe, A simulation study of the self-assembly of coarse-grained skin lipids, *Soft Matter*, 2012, **8**, 4802–4814.
31 D. N. LeBard, B. G. Levine and P. Mertmann, Self-assembly of coarse-grained ionic surfactants accelerated by graphics processing units, *Soft Matter*, 2012, **8**, 2385–2397.
32 *Monte Carlo and Molecular Dynamics Simulations in Polymer Science*, ed. K. Binder, Oxford University Press, New York, 1995.
33 R. G. Larson, Q. Zhou, S. Shanbhag and S. J. Park, Advances in polymer melt rheology, *AIChE J.*, 2007, **53**, 542–548.
34 *Modeling and Simulation in Polymers*, ed. P. D. Gujrati and A. I. Leonov, Wiley-VCH, 2010, ch 2.
35 K. Kremer, G. S. Grest and I. Carmesin, Crossover from rouse to reptation dynamics: a molecular dynamics simulation, *Phys. Rev. Lett.*, 1988, **61**, 566–569.
36 I. Carmesin and K. Kremer, The bond fluctuation method: a new effective algorithm for the dynamics of polymers in all spatial dimension, *Macromolecules*, 1988, **21**, 2819–2823.
37 R. B. Pandey, H. Heinz, J. Feng and B. L. Farmer, Bio-functionalization and immobilization of a membrane *via* peptide binding (CR3-1, S2) by a Monte Carlo simulation, *J. Chem. Phys.*, 2010, **133**, 095102–095108.
38 R. S. Hissam, B. L. Farmer and R. B. Pandey, Scaffolding of an antimicrobial peptide (KSL) by a scale-down coarse-grained approach, *Phys. Chem. Chem. Phys.*, 2011, **13**, 21262–21272.
39 J. Feng, R. B. Pandey, R. J. Berry, B. L. Farmer, R. R. Naik and H. Heinz, Adsorption mechanism of single amino acid and surfactant molecules to Au {111} surfaces in aqueous solution: design rules for metal binding molecules, *Soft Matter*, 2011, **7**, 2113–2120.
40 G. Collier, N. Vellore, J. Yancey, S. Stuart and R. Latour, Comparison between empirical protein force fields for the simulation of the adsorption behavior of structured LKpeptides on functionalized surfaces, *Biointerphases*, 2012, **7**, 1–19.
41 F. Iori, R. Di Felice, E. Molinari and S. Corni, GolP: an atomistic force-field to describe the interaction of proteins with Au (111) surfaces in water, *J. Comput. Chem.*, 2009, **30**, 1465–1476.
42 C. R. Herbers, K. Johnston and N. F. A. van der Vegt, Modelling molecule–surface interactions-an automated quantum-classical approach using a genetic algorithm, *Phys. Chem. Chem. Phys.*, 2011, **13**, 10577–10583.
43 J. Katoch, S. N. Kim, Z. Kuang, B. L. Farmer, R. R. Naik, S. A. Tatulian and M. Ishigami, Structure of a peptide adsorbed on graphene and graphite, *Nano Lett.*, 2012, **12**, 2342–2346.
44 J. C. Phillips, R. Braun, W. Wang, J. Gumbart, E. Tajkhorshid, E. Villa, C. Chipot, R. D. Skeel, L. Kalé and K. Schulten, Scalable molecular dynamics with NAMD, *J. Comput. Chem.*, 2005, **26**, 1781–1802.
45 C. Rajesh, C. Majumder, H. Mizuseki and Y. Kawazoe, A theoretical study on the interaction of aromatic amino acids with graphene and single walled carbon nanotube, *J. Chem. Phys.*, 2009, **130**, 124911.
46 M. Zhang, B.-C. Yin, X.-F. Wang and B.-C. Ye, Interaction of peptides with graphene oxide and its application for real-time monitoring of protease activity, *Chem. Commun.*, 2011, **47**, 2399–2401.